

Two-Step Preaging of an Al–Mg–Si Alloy

Zi Yang, Junjie Cheng, Zeqin Liang, and John Banhart*

Preaging (PA) is an industrial routine that suppresses the deleterious effect of natural aging and enhances the final paint-bake hardening of 6XXX aluminum alloys. In view of the different advantages of PA at high and low temperatures, the effects of performing PA in two steps at different temperatures, namely, 80 and 160 °C, are explored. Various two-step PA combinations are investigated, involving both the temperature orders and various aging times at both temperatures, while aiming at the same hardness after all PA treatments. These results are interpreted on the basis of cluster formation and vacancy evolution during two-step PA. In particular, the first PA step is found to play a more important role than suggested by the durations of the two PA steps as the clusters formed in the first step can strongly influence the subsequent evolution of both clusters and vacancies in the second step. It is found that two-step PA results in a compromise between the effects of one-step PA at both temperatures, that is, the enhancement of natural secondary aging stability is accompanied by a reduced paint-bake hardening or vice versa.

from solution heat treatment, but before storage at “room temperature.” PA enhances the strength of the alloys only moderately, but suppresses the subsequent natural secondary aging (NSA) hardening and, hence, prevents the compromised PB hardening response.^[4] It has been found by atom probe tomography that clusters formed during PA are compositionally close to the precipitates formed during PB, which is thought to facilitate the cluster-to-precipitate transition.^[5–7]

The effect of PA, that is, stabilizing the alloy at “room temperature” and avoiding sluggish or no strength increase during PB, depends on the exact aging parameters, namely, time and temperature. Saga et al.^[8] claimed that the PA temperature has to be higher than ≈ 70 °C not to compromise the following PB hardening. Birol et al.^[9] found that PA at low temperatures for short times

is inadequate for preventing the negative effect of NSA. Takaki et al.^[10] showed that PA at a higher temperature for the same time stabilizes the alloy during room-temperature storage for a longer time. Recently, the current authors systematically examined the effect of a large number of PA conditions covering a matrix of time and temperature combinations and found that the advantageous effect of PA is generally enhanced by pre-aging the alloy to higher hardness (or strength).^[11] Furthermore, when PA hardness is limited, such as that required by the sheet-forming process, the temperature of PA matters when comparing the same PA hardness increment. It was found that lower PA temperature ensures a higher stability of the alloy during NSA, whereas a higher PA temperature favors a higher PB hardening potential.^[11] Thus, the PA temperature can be used to tune the desired alloy properties, which are related to the types of clusters formed and the vacancy site fractions at different temperatures.


In most of the literature works, laboratory PA is conducted in a single-isothermal step right after solution heat treatment, but industrial practices are more complex than this. Alloys might undergo other “warm” treatments before PA, for example, acid washing, and after PA, the material is often slowly cooled down,^[12,13] a process which can last for hours and the microstructure might still vary. Some of those details are hard to reproduce under laboratory conditions and the effects of them are often unknown or partially ignored. To move closer to reality, we now include two PA steps at different temperatures. We vary the fractions of the steps while ensuring that the total hardness achieved after all PA remains constant at a level acceptable for the ensuing sheet forming process. Aging in both the steps is isothermal and, therefore, the conditions are still a clear

1. Introduction

Al–Mg–Si alloys are a class of age-hardenable alloys that find extensive applications in automotive industry for lightweighting of vehicles.^[1] The practical processing of such alloys involves a series of aging stages at various temperatures, during which the strength in service is achieved. The main and final strengthening effect is obtained in the paint-bake (PB) step through formation of fine precipitates. Unfortunately, alloys can already harden during room-temperature storage by the formation of solute clusters,^[2] which gives rise to a detrimental influence on the subsequent PB hardening, a phenomenon usually called “negative effect” of natural aging (NA).^[3] An industrial routine to mitigate this effect is to apply an additional aging stage at intermediate temperature, termed “preaging (PA),” after quenching

Z. Yang, J. Cheng, J. Banhart
Institute of Applied Materials
Helmholtz-Centre Berlin
Hahn-Meitner-Platz 1, 14109 Berlin, Germany
E-mail: banhart@helmholtz-berlin.de

Z. Liang
Novelis R&T Center
Rte des Laminoirs 15, 3960 Sierre, Switzerland

 The ORCID identification number(s) for the author(s) of this article can be found under <https://doi.org/10.1002/adem.202200973>.

© 2022 The Authors. Advanced Engineering Materials published by Wiley-VCH GmbH. This is an open access article under the terms of the Creative Commons Attribution License, which permits use, distribution and reproduction in any medium, provided the original work is properly cited.

DOI: 10.1002/adem.202200973

simplification compared with any real industrial heat treatment. Nevertheless, this model experiment provides orienting information on the influence of a second-temperature step in PA. As one-step PA at different temperatures shows advantages in different aspects, namely, either high NSA stability or high PB hardening potential, another rationale of the current study is to explore whether both advantages can be combined by splitting PA at one temperature into two steps at two different temperatures. Similar hardness levels after the individual PA steps imply that in each case the remaining solute supersaturation is almost the same and its influence on NSA stability or PB hardening is negligible. Hence, we can focus on the effects of various two-step PA on the vacancy site fraction and the formation of PA clusters.

To investigate the microstructural changes in various PA steps, we applied electrical resistivity measurements due to their sensitivity to clustering in Al–Mg–Si alloys at different temperatures.^[14] Moreover, differential scanning calorimetry (DSC) was used to indirectly probe the structure after various PA conditions as the evolution of the clusters formed at different temperatures during subsequent DSC (involving linear heating) causes distinct signals.^[11] Hardness testing was used to follow the NSA hardening kinetics and PB hardening of the alloys after various PA treatments. As cluster formation during NA is known to be dependent on the vacancy site fraction, and such information is experimentally hard to access, we simulated vacancy annihilation kinetics to obtain additional insights into the level of vacancy site fraction after various PA treatments.

2. Experimental Section

2.1. Material and Heat Treatments

A commercial alloy AA6014 was used in this study containing 0.65% Mg, 0.60% Si, 0.18% Fe, 0.08% Mn, and 0.12% Cu in weight. Solution heat treatment was performed at 540 °C for 1 h in an air circulation furnace or a vertical drop furnace in argon atmosphere, after which the samples were quenched in ice water and a hardness of ≈ 44.5 HBW was obtained. PA was conducted either in a single step in an oil bath at 80 or 160 °C, or in two steps first at 80 °C and then 160 °C, or vice versa. The two PA temperatures, namely, 80 and 160 °C, were chosen as the previous study suggests that their influence on subsequent NSA and PB hardening is distinct.^[11] PA was conducted such that an isohardness level of ≈ 65 HBW was reached in all the preaged samples. For two-step PA treatments, samples were aged in the first step to ≈ 50 or ≈ 60 HBW and then to the final hardness in the second step. The hardness increments (and thus aging times) of both the aging steps were varied simultaneously. The times required to achieve the desired hardness increments in two-step PA were determined in run-up experiments and are summarized in **Table 1**. The hardness increments in different stages of PA are visualized in the inset of **Figure 1**. NSA was conducted at 20 °C in a Peltier-cooled incubator, and after various NSA times, PB was carried out in an oil bath at 180 °C for 30 min. A schematic overview of the heat treatment temperature profile is given in **Figure 1**.

Table 1. Parameters of the PA conditions in the current study. “H” and “L” stand for high and low temperatures, respectively, and the numbers for modifications of treatments “H” and “L”.

Conditions	First-step PA	Second-step PA
H (Reference)	160 °C/15 min	–
H1	160 °C/10 min	80 °C/480 min
H2	160 °C/5 min	80 °C/930 min
L (Reference)	80 °C/960 min	–
L1	80 °C/480 min	160 °C/5 min
L2	80 °C/30 min	160 °C/13 min

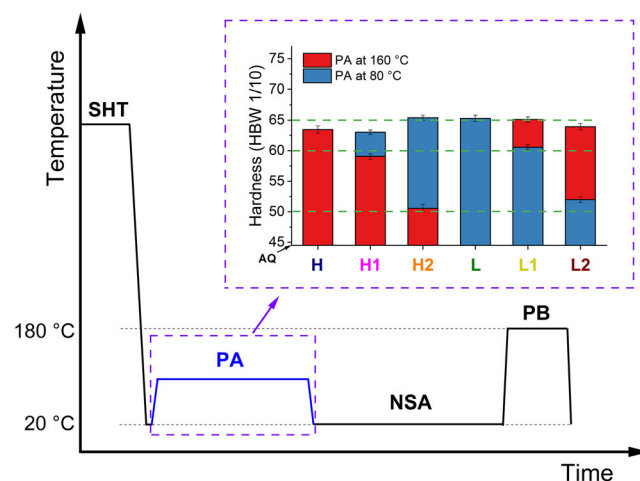


Figure 1. Schematic plot of the heat treatment program applied to the alloy. Inset shows the hardness increments during the various one-step or two-step PA treatments at different temperatures, AQ indicates the hardness level in the as-quenched state, and the horizontal lines are the three nominal target hardness values that were defined.

2.2. Methods

Hardness measurements were performed on the Qness 60 M hardness tester using 10 kgf load, an indenter of 1 mm diameter, and square-shaped alloy plates (10 mm × 10 mm × 10 mm). On each sample, eight indentations were made and the average and standard deviations were calculated. DSC measurements were performed on the Netzsch DSC F204 Phoenix unit from 0 to 400 °C at a heating rate of 10 K min^{−1} using disks of 4.8 mm diameter and 1 mm thickness and a pure Al sample of similar mass as a reference. The signal of an immediate rerun after the measurement was used to correct the baseline.^[11,15] Electrical resistivity was measured on coiled alloy wires of 0.67 mm diameter and 600–800 mm length after aging at 80 or 160 °C for various times and quenching to liquid nitrogen (−196 °C). The four-point probe method was applied at a constant current of 100 mA.

Vacancy site fraction evolutions during quenching and various PA steps were simulated using the MatCalc 6 software that uses the FSAK vacancy annihilation/generation model^[16] and considered two types of vacancy sources and sinks, namely, grain boundaries and dislocation jogs. An experimentally measured grain diameter of 25 μm^[17] was applied in the simulation, as well

as an approximated dislocation density of 10^{11} m^{-2} for annealed metal and a jog spacing number of 50. These parameters were later varied to explore their influence on the simulated vacancy site fractions. The interactions between vacancies and solutes/clusters were not implemented in the simulation, because their interaction energies were either too low to have a pronounced impact (vacancy–Mg, Si) or not available (vacancy–cluster). Therefore, its influence on the vacancy dynamics could only be qualitatively discussed. The quenching rate in water was assumed to be -1000 K s^{-1} (linear), while heating or cooling in oil (between different PA steps) took place at $\pm 100 \text{ K s}^{-1}$.

3. Results

3.1. Hardness

The hardness of the alloy after PA is stable during NSA for some time, after which it increases, as shown in **Figure 2a**. Such times range from several days to several weeks depending on the PA condition applied. This defines the NSA stability of the alloy after PA, but due to the measurement error, a precise determination of the time at which hardness starts to increase is difficult. An indirect way to compare the NSA stabilities is to compare the time needed during NSA to reach the same hardness, for example, 70 HBW. Faster hardening during NSA implies lower stability. Accordingly, the PA conditions are divided into the three groups, namely, “H” and “H1” with the lowest NSA stability, “H2” and “L2” with an intermediate stability, and “L” and “L1” with the highest stability. As the aging time at 160 °C decreases in the first step of PA and the aging time at 80 °C increases in the second step of PA (“H1”→“H2”), the alloy becomes more stable during NSA storage. In turn, increasing the fraction of aging at 160 °C in the second step of PA (“L1”→“L2”) makes the alloy less stable during NSA. Notably, PA treatment with a short second step does not obviously change the NSA stability compared with its one-step PA reference (compare “H” vs “H1” and “L” vs “L1”).

The conditions of PA also influence the hardness after further PB. If PB is directly applied after PA with almost no intermediate NSA—first points as shown in **Figure 2b**—samples preaged in

the first step at 160 °C (“H1” and “H2”) show higher PB hardness than those samples preaged in the first step at 80 °C (“L1” and “L2”). As NSA progresses, the hardness of the NSA + PB state first remains constant but then decreases after a certain degree of NSA has been reached. The time of uncompromised PB hardness is the shortest for PA conditions “H” and “H1,” longer for PA conditions “H2” and “L2,” and longest for PA conditions “L1” and “L,” where the decrease of PB hardness after 6 months of NSA is very small.

3.2. Electrical Resistivity

An electrical resistivity of $1339 \pm 11 \text{ n}\Omega \text{ cm}$ at $-196 \text{ }^\circ\text{C}$ is obtained after quenching the alloy from the solutionizing temperature. During the various aging treatments, different electrical resistivity evolutions are observed (**Figure 3**). Isothermal

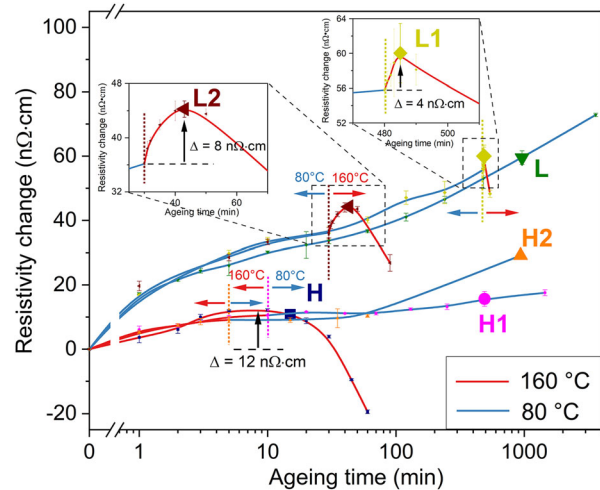


Figure 3. Change of electrical resistivity during aging at 160 and 80 °C, as well as during various two-step aging treatments measured after interrupting ageing in liquid nitrogen. Aging steps at different temperatures are displayed in different line colors, with the transitions marked by vertical dotted lines. The states defined in Table 1 are labeled accordingly and feature enlarged symbols. Insets show stages of pronounced changes.

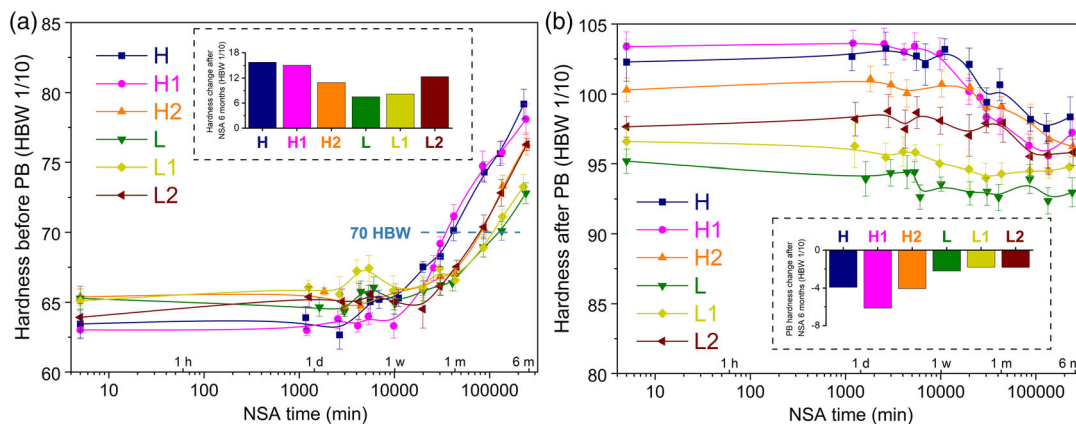


Figure 2. Hardness of the alloy after various PA treatments and a) NSA and b) NSA + PB as a function of NSA time. Insets show the property change after 6 months of NSA.

aging at 80 °C increases the resistivity monotonically within the time of measurement (≈ 3500 min), whereas the resistivity during aging at 160 °C is increased in the first 10 min and later reduced rapidly. The resistivity increase during aging at 80 °C is also much more pronounced than at 160 °C.

If aging is performed in two steps, resistivity evolution in the second step deviates from the trend of the first step and exhibits some features of direct ageing at that temperature. Switching from 80 to 160 °C gives rise to a resistivity maximum, while ageing at 80 °C after 160 °C further increases resistivity, eventually beyond the level achievable by direct ageing at 160 °C. The change of resistivity in the second step is also influenced by the time of the first step. By increasing the time of aging at 80 °C in the first step from none (“H”) to 480 min (“L1”), a decline in the maximum resistivity increase is seen in second-step aging at 160 °C (from 12 to 4 $n\Omega\cdot\text{cm}$ as shown in Figure 3). A longer time of aging at 160 °C before 80 °C also results in a slower resistivity increase at 80 °C. In conclusion, as the time of the first step gets longer, the change in the second step decreases.

3.3. Differential Scanning Calorimetry

DSC traces measured after various PA are shown in Figure 4a. Several exothermic peaks are observed: peaks 1–4 at ≈ 220 , ≈ 250 , ≈ 265 , and ≈ 290 °C, respectively. The heights of the peaks vary with the PA conditions. Reference sample “H” shows the highest peak 1 and hardly any indication of peak 3, whereas sample “L” shows the lowest peak 1 and the most pronounced peak 3. Compared with “H,” two-step preaged samples, regardless of whether aging at 80 °C is placed before 160 °C (“L1” and “L2”) or after 160 °C (“H1” and “H2”), show a similar trend, that is, peak 1 reduced and peak 3 enhanced (Figure 4b). Peaks 2 and

4 are also influenced, but the change is minor. In turn, if aging at 160 °C partially replaces PA at 80 °C, peak 1 builds up and peak 3 shrinks (Figure 4c). Generally, a higher fraction of such replacement strengthens the change of the DSC peaks, such as “H2” compared with “H1.” However, it is also found that replacing the first step has much higher impact than the second step although the hardening effects during PA are similar, for example, “H1” compared with “L2.”

4. Discussion

4.1. Cluster Formation During Two-Step Preaging

Cluster formation has been characterized by changes in various physical properties of the alloy, most prominently hardness and electrical resistivity. Cluster hardening has been reported to be linearly related to the released heat of cluster formation, which can be considered a first approximation proportional to the volume fraction of clusters.^[18,19] Therefore, PA to the same hardness level implies that similar fractions of clusters are formed. In contrast, electrical resistivity reacts to cluster formation in a more complicated way, where many factors such as the size distribution of the clusters influence the electrical resistivity, and these have to be taken into comparison with the initial solid solution. The initial anomalous resistivity increase is thought to be caused by increased electron scattering by the clusters formed,^[20] where a critical size of clusters is found associated with the resistivity maximum of Al–Zn alloys during aging.^[21] Using the cluster information obtained by 3D atom probe tomography, Esmaili et al.^[22] further clarified that the number density of the clusters has an eminent role in the resistivity maximum at various aging temperatures, that is, the higher resistivity maximum during

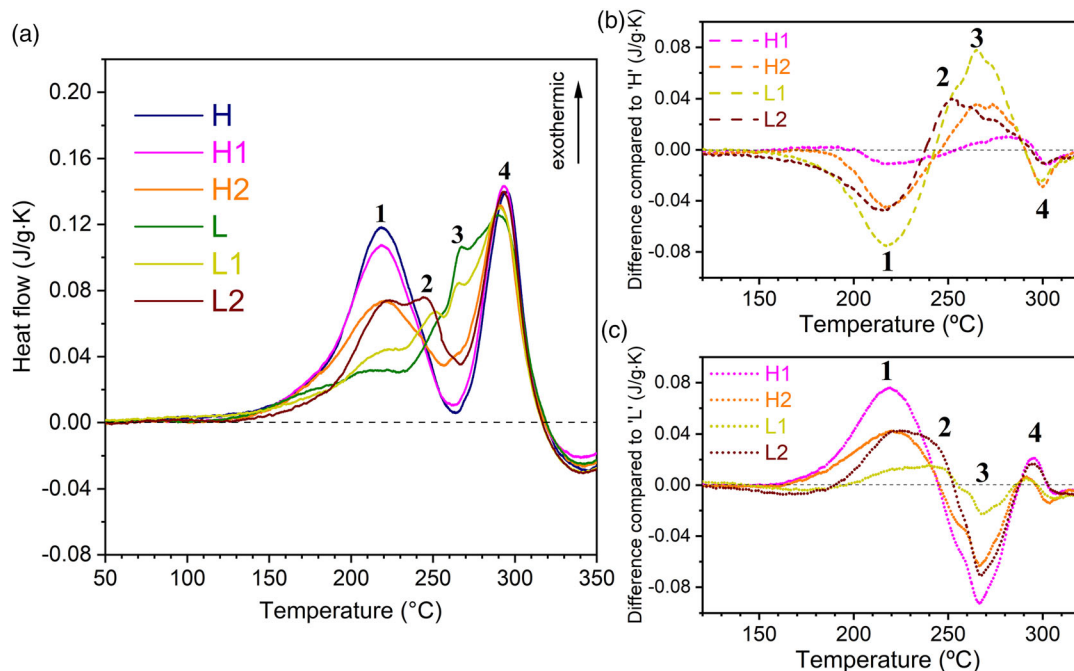


Figure 4. a) DSC traces after various one- and two-step PA treatments carried out at a heating rate of 10 K min^{-1} . Numbers refer to various exothermic peaks. b, c) Differences of the DSC traces of two-step preaged samples compared with b) “H” and c) “L”.

aging at lower temperature is associated with a higher number density of clusters, which confirms the earlier claims of Panseri et al.^[23]. Given that a much higher electrical resistivity is observed in “L” than in “H,” it is, therefore, inferred that more but possibly smaller solute clusters are present in “L” than in “H.”

With this information in mind, we can qualitatively interpret the cluster evolution during two-step PA by correlating the resistivity change with hardness change in the various aging steps, as shown in **Figure 5**. Similar plots have been used by Kim et al.^[24] to interpret cluster evolution during natural aging of Al–Mg–Si alloys and by Salazar–Guapuriche et al.^[25] to explain the precipitation in an Al–Zn–Mg–Cu alloy at various temperatures and aging stages. The main argument is that a high slope (mainly hardness change) is primarily caused by the growth of clusters, while a low slope (mainly resistivity change) indicates a rise in the number density of clusters. For example, in “H1” and “H2,” where aging is first at 160 °C and then 80 °C, the slope of the second step is lower than that of “H” in the same step (Figure 5a), which indicates a higher number density of clusters formed compared with “H”. The slope of that step (80 °C) is, however, also higher than the slope of isothermal aging at

80 °C (“L”) from the as-quenched state to the same hardness increase, suggesting fewer clusters formed compared with the independent formation of new clusters. Such a difference might be a result of some solutes attaching to the clusters previously formed at 160 °C, leading to the growth of these clusters. Similar conclusions can be drawn for “L1” and “L2” (Figure 5b).

This finding is indirectly supported by the DSC traces (Figure 4). The various exothermic peaks can be interpreted as a complex scenario involving precipitation of various types of phases that are either newly formed in the matrix or transformed from already existing PA clusters during linear heating. Among the four peaks, peak 4 is understood as the formation of β' phase,^[26,27] while the interpretation of peaks 1–3 is more complicated. Takaki et al.^[10] observed two peaks in the range of ≈ 230 – 270 °C in the preaged alloy and argued that the first peak is related to β'' precipitation resulting from a transformation of PA clusters, while the second peak reflects β'' precipitation in the matrix that takes place after the dissolution of NA clusters, as they found that NSA promotes the second peak and suppresses the first peak. Although our DSC curves show three peaks, Takaki’s interpretation still coincides with our results as the differences between different PA conditions mainly concern two peaks, namely, peaks 1 and 3 (Figure 4b,c). There is also a small change for peak 2, but it is much less pronounced compared with peak 3. In previous work,^[11] we find that the DSC trace of a naturally aged alloy shows a very pronounced β'' precipitation signal at a position near that of peak 3 in this work, which is also in line with Takaki’s interpretation. It is inferred that PA at lower temperature induces more clusters similar to NA clusters that are hard to directly transform into β'' , which is expected to cause a lower peak 1 and a higher peak 3. This is indeed the observed trend in all the DSC curves: as hardening during aging at 80 °C increases (“H” \rightarrow “H1” \rightarrow “H2” or “L2” \rightarrow “L1” \rightarrow “L”), peak 1 shrinks, while peak 3 grows (Figure 4b,c). However, the exact change of the peaks is not only related to the hardening fractions at various temperatures but also the temperature sequence. For instance, the hardness increment at 80 °C in “H2” (starting with 160 °C) is much higher than in “L2.” Therefore, one would expect a lower peak 1 and a higher peak 3 in the DSC trace of “H2,” but the experimental DSC traces of “H2” and “L2” show very similar peak amplitudes. This shows that the first step has a larger influence than suggested by the hardness increment during PA and implies that clusters formed in the first step further grow in the second step and, therefore, the cluster fractions of 160 and 80 °C in “H2” and “L2” are in fact more similar than the hardening fractions.

Altogether, these results suggest that during the second step of PA, the solutes partially attach to the preexisting clusters and partially form new clusters, likely in the space between these pre-existing clusters.

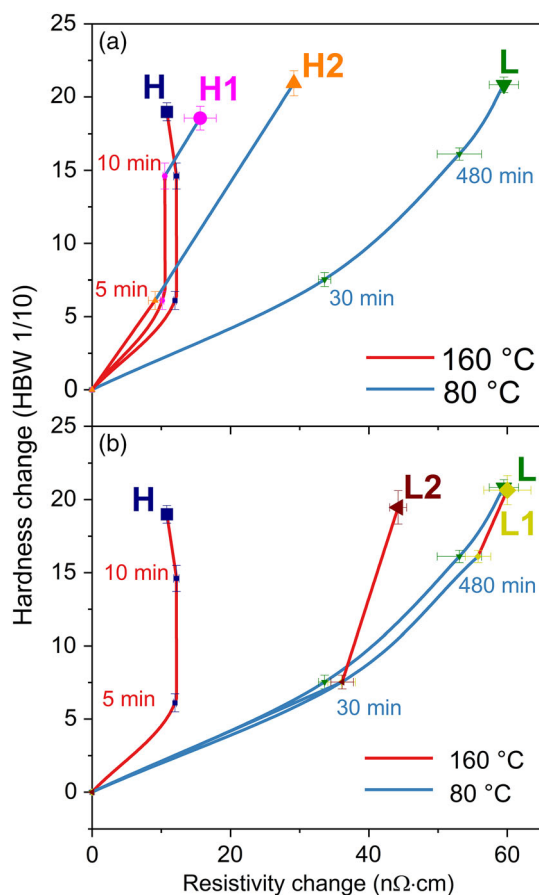


Figure 5. Hardness change as a function of resistivity change during various one- and two-step PA treatments. a) Comparison of “H”–“H1”–“H2”–“L”. b) Comparison of “H”–“L1”–“L2”–“L”. Resistivity data are taken from Figure 3. The hardness data for the intermediate points of “H” and “L” are taken from Figure 1, which is similar to previous work.^[32]

4.2. Influence of Two-Step PA on Subsequent Clustering and Precipitation

4.2.1. Natural Secondary Aging

Vacancies play a central role for the diffusion of substitutional solutes and, hence, the kinetics of precipitation in Al–Mg–Si

alloys. NA is known to be dependent in particular on excess vacancies.^[28] After PA, an equilibrium vacancy site fraction (or higher) at that temperature can be reached, but it is still orders of magnitude higher than the equilibrium site fraction at room temperature, which is the reason why notable NSA clustering can still take place and an associated hardness change observed. As the solute supersaturations after various PA are considered all similar due to the same PA hardness level, vacancies are expected to determine the differences in NSA kinetics. Knowing the vacancy site fractions after various PA treatments are, therefore, important for understanding the NSA hardening kinetics. As the evolution of vacancy site fraction during PA is a dynamic process and experimentally difficult to measure, we calculate the vacancy site fraction during and after various one- and two-step PA using the software MatCalc and FSAK vacancy kinetics.^[16]

Figure 6 shows the simulated vacancy site fractions during quenching and various aging treatments. Vacancies are partially lost in the first short period of quenching when the temperature is still high, whereas they are quenched in later and are largely preserved. During aging, the vacancy site fraction evolves toward the equilibrium level. It takes about 90 s to reach the equilibrium site fraction at 160 °C and 3000 s at 80 °C. This is fast enough to ensure that in all the two-step preaged conditions, the equilibrium vacancy site fraction of the end temperature has been reached, namely, with values in “H” identical with “L1” and “L2,” and in “L” identical with “H1” and “H2.” However, this does not comply with the NSA hardening kinetics measured after different PA conditions, where a short second step hardly influences NSA hardening (Figure 2a: H/H1 and L/L1 are very similar). Clearly, there is a discrepancy between the results of the simulations and the NSA hardness curves that require further detailed examination.

First, it is known that the clustering kinetics during NSA is not necessarily proportional to the vacancy site fractions after PA. One example is the NSA kinetics after PA at various temperatures for long times, where equilibrium vacancy site fractions are assumed to have been achieved after PA. NSA hardening differences are, however, much smaller than the spread of the equilibrium vacancy site fraction.^[11] Another example is NA hardening after quenching from the solutionizing temperature at various rates. Vacancy site fractions before NA are determined to be 1–2 orders of magnitude apart, but the NA hardening rates differ only in the first ≈ 100 min.^[29] In both examples, the vacancy differences are narrowed down in the clustering kinetics, but still they do not explain the very different NSA hardening kinetics if the same vacancy site fractions are achieved according to the simulations (e.g., “H” and “L1”). Therefore, it is more likely that the vacancy simulations are incorrect, that is, vacancy evolution should be much slower than calculated.

Simulations are dependent on the choices of the parameters and models. We have not taken into account other types of vacancy sinks and sources such as Frank loops, which would yield even faster vacancy kinetics, thus bringing us even farther away from explaining the scenario. Changing input parameters such as the grain diameter or dislocation density (the jog fraction has a similar effect) would slow down the kinetics only when both are markedly changed (**Figure 7**), but such a proposition leads to unrealistically large grain diameters that are in contradiction to our experimentally observed value or low dislocation jog densities.

The vacancy dynamics earlier considers only the aspects from the number density of sinks and sources of vacancies, but it can also be influenced by how vacancies reach them, which is indeed a complex process. In a simplified scenario,^[30] a vacancy can meet a solute atom on its “random walk” through the matrix

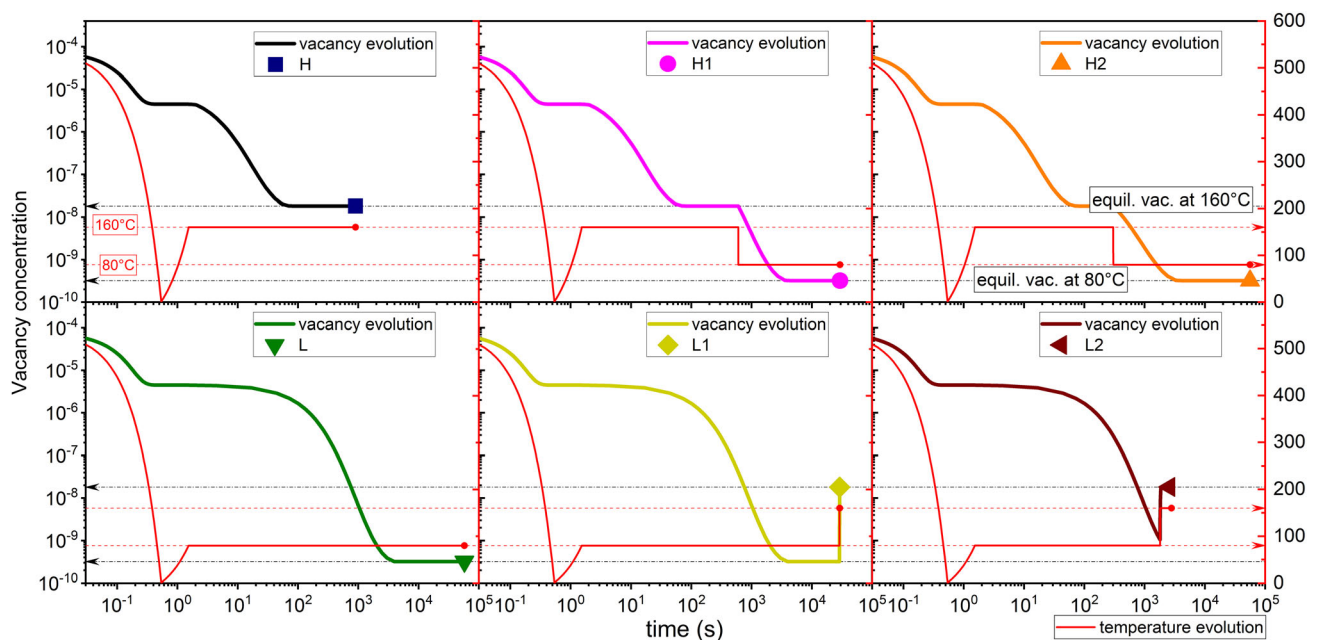


Figure 6. Simulated evolution of vacancy site fraction during quenching and various PA treatments. Horizontal broken lines show the two aging temperatures and their equilibrium vacancy site fractions.

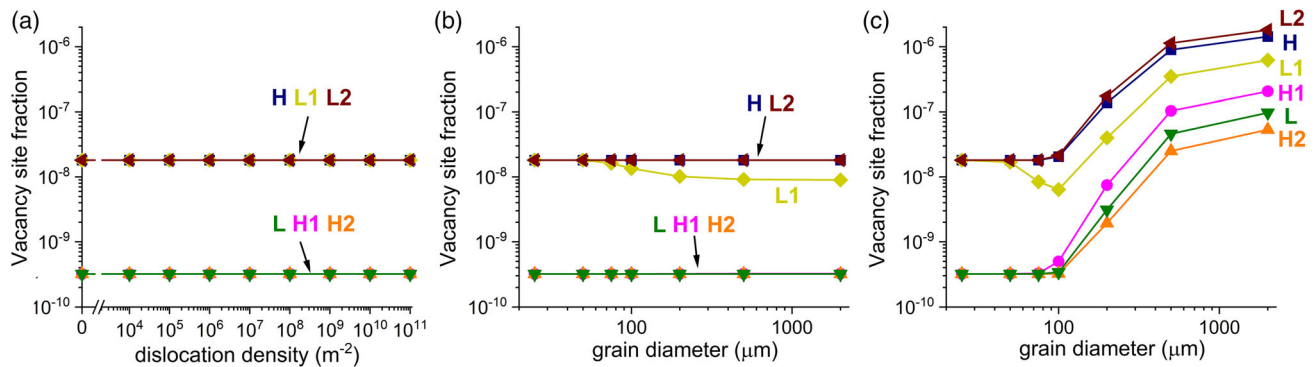


Figure 7. Simulated final vacancy site fractions after solutionizing, quenching, and various subsequent PA treatments as a function of a) varying dislocation density ($\leq 10^{11} \text{ m}^{-2}$) at a constant grain diameter of $25 \mu\text{m}$, b) varying grain diameter ($\geq 25 \mu\text{m}$) at a constant dislocation density of 10^{11} m^{-2} , and c) varying grain diameter ($\geq 25 \mu\text{m}$) at a constant dislocation density of 10^{10} m^{-2} .

and move jointly until the vacancy either departs from the solute atom or the couple encounters another solute or a solute cluster and the vacancy departs. Whenever a vacancy binds with a solute or a cluster, its walk becomes not random since the probabilities of jumping to the nearest sites are not all equal due to the interaction with the solute/cluster and the vacancy can be temporarily trapped. Such trapping depends on the interaction energy between the vacancy and the object at which it is trapped. This energy is low between a vacancy and a solute atom (Mg or Si),^[31] but presumably much higher between a vacancy and a solute cluster.^[30] Therefore, a vacancy spends a longer time with a cluster before continuing the “random walk” again in the matrix and eventually encounters a sink. Likewise, vacancies generated by sources might also be temporarily trapped by the clusters on the way to replenishing the vacancy reservoir in the matrix. This mechanism delays vacancy evolution without changing the density of vacancy sinks and sources. Moreover, since such interaction is expected to be stronger as clustering progresses, it affects the late stage of aging more than the initial step. Therefore, during initial PA, equilibrium can still be reached in a short time when there are few clusters present, but the transition to a second temperature requires much longer time for the new equilibrium vacancy site fraction to be achieved. As the first PA step gets shorter (fewer clusters formed), for example, “H1”→“H2,” vacancy evolution is delayed less in the second-step PA and, thus, NSA hardening is modified more and now closer to “L.” In this way, the subsequent NSA hardening after various PA can be qualitatively explained.

4.2.2. Paint-Bake Hardening

Hardness after PB is determined by both PA and NSA. For a given PA condition, the PB hardness is compromised by prolonged NSA. This is linked to the formation of NA clusters and gives rise to the so-called “negative effect.” Therefore, an earlier negative effect is usually observed when NSA stability is lower. As this property, as discussed in the previous section, also depends on the PA condition, PB hardness after NSA is, therefore, indirectly influenced. A direct influence of PA treatment on PB hardness lies in the PB hardening potential when no NSA is applied. One-step PA at $160 \text{ }^\circ\text{C}$ (“H”) and $80 \text{ }^\circ\text{C}$ (“L”) shows very distinct PB hardening, which was argued to be related to the ability of PA clusters transforming into hardening precipitates, possibly associated with the Mg/Si ratios of the clusters formed at two individual temperatures and the different crystal structures of the cluster.^[11] Since two-step preaged alloy contains clusters independently formed at both temperatures as derived from the resistivity measurements (Section 4.1), it is understandable that the PB hardening potential lies between that of the two one-step PA treatments.

shows very distinct PB hardening, which was argued to be related to the ability of PA clusters transforming into hardening precipitates, possibly associated with the Mg/Si ratios of the clusters formed at two individual temperatures and the different crystal structures of the cluster.^[11] Since two-step preaged alloy contains clusters independently formed at both temperatures as derived from the resistivity measurements (Section 4.1), it is understandable that the PB hardening potential lies between that of the two one-step PA treatments.

4.2.3. Importance of Temperature Sequence

Two-step PA does not fully combine the advantages of high PA temperature (high PB hardenability) and low PA temperature (high NSA stability), but rather a mixture of the two behaviors. Functionally, it is approximately equivalent to the one-step PA at an intermediate temperature. The reason for this is that high NSA stability requires long aging at low temperature in the second step to reach a state of lower vacancy site fraction, but a high PB hardening response requires long aging at high temperature to ensure a cluster configuration favorable for precipitation. Thus, these two demands are contradictory to each other, and it is questionable whether the advantages of different PA temperatures can be simply combined.

Still, some new understandings of multistage aging in Al–Mg–Si alloys are gained such as the importance of the temperature sequence. For instance, “H2” and “L1” show hardening during PA at different temperatures in a symmetrical way, namely, hardening at the same temperatures is the same but in different orders, but their NSA stability and PB hardenability are different (Figure 2). Two-step PA is dominated more by the first step than the second. Similar results can be found in “H2” and “L1.” The interpretation for a greater impact of the first step is that the clusters formed there can further grow, as well as affect the vacancy evolution in the second step. Also, as the first step follows quenching from solutionizing, where a high excess vacancy site fraction is present, it usually takes a relatively short time to give rise to a pronounced clustering. For industrial practice, this implies that the alloy needs to enter the desired PA temperature quickly to minimize the unwanted impact of prior aging. Moreover, since the second step needs to be long

to change the behavior of the alloy, cooling after PA does not require a high rate after solutionizing. Instead, slow natural cooling can be even used to provide some extra PA hardening, thus higher NSA stability, without extra energy input. This justifies industrial practice where PA of alloy sheet material is conducted in a continuous furnace after solutionizing and quenching, which constitutes a first PA step, after which the sheets are coiled and left to cool to “room temperature,” which can be seen as a second PA step at a lower, however slowly decreasing temperature, especially in the coil center. Because this second step of PA has a less pronounced effect—as shown here—the sheets do not have to be uncoiled anymore, which is a processing advantage.

5. Conclusion

Cluster formation during two-step PA at two different temperatures and its effect on the subsequent NSA and PB hardening have been investigated and compared with those of one-step PA, while maintaining the boundary condition that similar hardness levels after various PA treatments are reached. The following conclusions can be drawn. 1) One-step isothermal PA at 160 °C (sample “H”) results in a higher PB hardening potential, while PA at 80 °C (sample “L”) ensures a higher stability of the alloy during subsequent NSA in accordance with a previous study. 2) By partially replacing the PA of sample “H” with aging at 80 °C with a large part in the second step (“H2”), or in the first step (“L1” and “L2”), the PB hardening potential is lowered, while the NSA stability is enhanced with respect to “H,” that is, the effect of two-step PA is a compromise of the properties of “H” and “L.” This also applies to “L” and its counterparts, but the effect is reversed. 3) Although two-step PA combines the effects of PA at both the temperatures, the first-step PA plays a more important role: a short second aging step has little influence on subsequent PB hardening and NSA stability (“H”→“H1” and “L”→“L1”). “H2” and “L2” show similar behavior, although their hardness increments at 160 °C and 80 °C are very different. 4) The effects of two-step PA can be understood via the cluster and vacancy evolutions in the two aging steps. Cluster formation in the second step is characterized via the electrical resistivity and DSC measurements as a process involving both the growth of clusters formed in the first step and independent clustering. The vacancy site fraction evolves toward the thermal equilibrium in the second aging step, but the progress is retarded by the interaction between clusters and vacancies. Therefore, the long-lasting influence of the clusters formed in the earlier stage explains the higher importance of the first step for two-step PA.

Acknowledgements

Open Access funding enabled and organized by Projekt DEAL.

Conflict of Interest

The authors declare no conflict of interest.

Data Availability Statement

The data that support the findings of this study are available from the corresponding author upon reasonable request.

Keywords

Al–Mg–Si alloys, preaging, precipitation, vacancies

Received: July 5, 2022

Revised: August 18, 2022

Published online:

- [1] J. Hirsch, *Mater. Trans.* **2011**, *52*, 818.
- [2] P. Dumitraschkewitz, S. S. A. Gerstl, L. T. Stephenson, P. J. Uggowitz, S. Pogatscher, *Adv. Eng. Mater.* **2018**, *20*, 1800255.
- [3] J. Banhart, C. S. T. Chang, Z. Q. Liang, N. Wanderka, M. D. H. Lay, A. J. Hill, *Adv. Eng. Mater.* **2010**, *12*, 559.
- [4] L. Zhen, S. B. Kang, *Scr. Mater.* **1997**, *36*, 1089.
- [5] A. Serizawa, S. Hirose, T. Sato, *Metall. Mater. Trans. A* **2008**, *39A*, 243.
- [6] M. W. Zandbergen, Q. Xu, A. Cerezo, G. D. W. Smith, *Acta Mater.* **2015**, *101*, 136.
- [7] O. Engler, C. D. Marioara, Y. Aruga, M. Kozuka, O. R. Myhr, *Mater. Sci. Eng. A* **2019**, *759*, 520.
- [8] M. Saga, Y. Sasaki, M. Kikuchi, Z. Yan, M. Matsuo, *Mater. Sci. Forum* **1996**, *217*, 821.
- [9] Y. Birol, *Mater. Sci. Eng. A-Struct.* **2005**, *391*, 175.
- [10] Y. Takaki, T. Masuda, E. Kobayashi, T. Sato, *Mater. Trans.* **2014**, *55*, 1257.
- [11] Z. Yang, Z. Liang, D. Leyvraz, J. Banhart, *Mater.* **2019**, *7*, 100413.
- [12] S. Q. Zhu, H. C. Shih, X. Y. Cui, C. Y. Yu, S. P. Ringer, *Acta Mater.* **2021**, *203*, 116455.
- [13] G. Li, M. Guo, J. Du, L. Zhuang, *Mater. Des.* **2022**, *218*, 110714.
- [14] C. Panseri, T. Federighi, *J. I. Met.* **1966**, *94*, 99.
- [15] R. Ivanov, A. Deschamps, F. De Geuser, *Acta Mater.* **2018**, *157*, 186.
- [16] F. D. Fischer, J. Svoboda, F. Appel, E. Kozeschnik, *Acta Mater.* **2011**, *59*, 3463.
- [17] Z. Yang, Study of the Effect of Thermal Pretreatments on the Artificial Ageing Response of 6xxx Al Alloys, Master thesis, RWTH Aachen **2016**.
- [18] Z. Yang, I. Erdle, C. H. Liu, J. Banhart, *J. Mater. Sci. Technol.* **2022**, *120*, 78.
- [19] M. J. Starink, L. F. Cao, P. A. Rometsch, *Acta Mater.* **2012**, *60*, 4194.
- [20] Z. Matyas, *Lond. Edinb. Dublin Philos. Mag. J. Sci.* **1949**, *40*, 324.
- [21] H. Herman, J. B. Cohen, *Nature* **1961**, *191*, 63.
- [22] S. Esmaili, D. Vaumousse, M. W. Zandbergen, W. J. Poole, A. Cerezo, D. J. Lloyd, *Philos. Mag.* **2007**, *87*, 3797.
- [23] C. Panseri, T. Federighi, *Acta Metall. Mater.* **1960**, *8*, 217.
- [24] S. N. Kim, J. H. Kim, H. Tezuka, E. Kobayashi, T. Sato, *Mater. Trans.* **2013**, *54*, 297.
- [25] M. A. Salazar-Guapuriche, Y. Y. Zhao, A. Pitman, A. Greene, *Mater. Sci. Forum* **2006**, *7010* 853.
- [26] I. Dutta, S. M. Allen, *J. Mater. Sci. Lett.* **1991**, *10*, 323.
- [27] G. A. Edwards, K. Stiller, G. L. Dunlop, M. J. Couper, *Acta Mater.* **1998**, *46*, 3893.
- [28] Z. Yang, J. Banhart, *Acta Mater.* **2021**, *215*, 117014.
- [29] Z. Yang, X. Jiang, X. Zhang, M. Liu, Z. Liang, D. Leyvraz, J. Banhart, *Scr. Mater.* **2021**, *190*, 179.
- [30] H. S. Zurob, H. Seyedrezai, *Scr. Mater.* **2009**, *61*, 141.
- [31] C. Wolverton, *Acta Mater.* **2007**, *55*, 5867.
- [32] Z. Yang, Z. Liang, D. Leyvraz, J. Banhart, *Data Brief.* **2019**, *27*, 104494.